Volume 8, Issue 3, 2018, 3203 - 3206 ISSN 2069-5837

Biointerface Research in Applied Chemistry

www.BiointerfaceResearch.com

Original Research Article Open Access Journal

Received: 22.05.2018 / Revised: 10.06.2018 / Accepted: 12.06.2018 / Published on-line: 15.06.2018

Supercritical antisolvent process phase equilibria in ternary systems: microparticles and nanoparticles precipitation

Stefano Cardea[1], Ernesto Reverchon[1], Iolanda De Marco[1,*]

[1]Università di Salerno, Dipartimento di Ingegneria Industriale, Via Giovanni Paolo II, 132 - 84084 Fisciano (SA), Italy

*corresponding author e-mail address: ***idemarco@unisa.it***

ABSTRACT

In this work, the jet break-up and the phases formation during the Supercritical Antisolvent (SAS) precipitation of different compounds were studied. Indeed, the formation of the different morphologies, such as expanded microparticles, microparticles, and nanoparticles can be obtained, varying the operating conditions. In order to observe some macroscopic aspects related to the process, a windowed SAS precipitator was used and the formation of one or more phases that influence the morphology of the powders was investigated. Two model compounds were precipitated, such as yttrium acetate and prednisolone.

Keywords: *supercritical carbon dioxide; nanoparticles; microparticles; high-pressure vapor-liquid equilibria; jet break-up.*

1. INTRODUCTION

The production of micro- and nano-particles with controlled particle size and particle size distribution is of great interest in several industrial fields. In alternative to traditional processes, some supercritical fluids based processes have been proposed. The most promising is semi-continuous Supercritical Antisolvent precipitation (SAS). It is based on the use of a supercritical antisolvent (CO_2 as a rule) that is added to the liquid solution and induces the fast precipitation of the solute that is not soluble in the antisolvent. SAS precipitation has been proposed to produce micrometric and submicrometric particles of various materials: explosives [1], polymers [2-4], biopolymers [5, 6], superconductor precursors and catalysts [7-9], and pharmaceutical compounds [10-14]. However, in several cases, precipitation was unsuccessful even when all process conditions were correctly selected on the basis of binary systems behavior. Therefore, some authors tried to develop a better understanding of the mechanisms controlling SAS. Droplet formation due to jet break-up and mass transfer between phases have been analyzed in some cases [15]. Until now, only a limited attention has been devoted to the thermodynamic aspects of the process [16]. The aim of this work is to use a windowed SAS precipitator to analyze some macroscopic aspects of the SAS process: mainly jet break-up and fluid phases' formation during the precipitation process. Particularly, we want to ascertain how the formation of one or more phases influences the morphology of the precipitated powders.

2. EXPERIMENTAL SECTION

The windowed SAS apparatus consists of two HPLC pumps (Gilson, mod. 305) used to deliver the liquid solution and supercritical CO_2. The pump that delivers the supercritical fluid (SCF) was modified for compressible fluids pumping adding a cooling head and modifying the inlet and the outlet valves. A vessel of 375 cm^3 I.V. has been used as precipitation chamber. It consists of a stainless steel cylinder with two quartz windows put along the longitudinal section of the chamber. The precipitator is electrically heated. The liquid solvent or the liquid mixture is delivered to the precipitator through a 60 μm diameter stainless steel nozzle. Supercritical CO_2 is delivered through another inlet port located on the top of the chamber. The pressure in the chamber is measured by a test gauge manometer (Salmoiraghi, mod. SC-3200) and regulated by a micrometering valve (Hoke, mod. 1315G4Y) located at the exit (bottom) of the chamber.

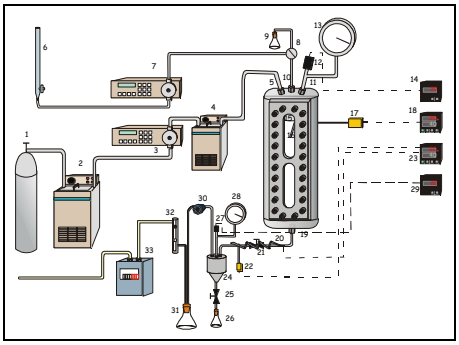

Figure 1. Schematic representation of the apparatus. 1), 6) CO_2 and liquid solution vessels; 2), 4) Cooling and heating devices; 3), 7) High pressure pumps; 5), 10) CO_2 and liquid solution inlet; 8) Three-way valve; 12), 17), 22), 27) Thermocouples; 13), 28) Manometers; 14), 29) Temperature detectors; 15) Injection nozzle; 18), 23) Temperature controllers; 19) CO_2 and solvent output; 21) Micrometering valve; 24) Liquid separator; 25) On-off valve; 30) Backpressure valve; 32) Calibrated rotameter; 33) Dry test meter.

A stainless steel porous frit is put at the bottom of the chamber; it collects the solid product but allows the CO_2-organic solvent solution to pass through.

A second collection chamber located downstream the micrometering valve is used to recover the liquid solvent. The pressure in this chamber is regulated by a backpressure valve (Tescom, mod. 26-1723-44). At the exit of the second vessel, a rotameter and a dry test meter are used to measure the CO_2 flow rate and the total quantity of antisolvent delivered, respectively (Figure 1).

Yttrium acetate (YAc) and Prednisolone (PNS) with a purity of 99.9% and dimethyl sulfoxide (DMSO) and methanol (MeOH) with a purity of 99.9% were supplied by Sigma-Aldrich (Italy). CO_2 99.9% was given by Morlando Group (Italy). The approximate solubilities of YAc in DMSO and MeOH are 320 and 55 mg/mL, respectively; in the case of PNS in MeOH, the solubility is 50 mg/mL.

A SAS experiment begins by delivering supercritical CO_2 to the precipitation chamber until the desired pressure is reached. The antisolvent steady flow is then established. The pure solvent is sent through the nozzle to the chamber to obtain steady state composition conditions during the solute precipitation. The pure solvent is also delivered to avoid the closure of the injection nozzle due to the precipitation of solute inside it during the startup procedures. At this point, the flow of the liquid solvent is stopped and the liquid solution is delivered through the nozzle. The experiment ends when the delivery of the liquid solution to the chamber is interrupted. However, supercritical CO_2 continues to flow to wash the chamber to eliminate the residual content of the solvent solubilized in the supercritical antisolvent.

Samples of the powders precipitated on the metallic frit were observed by Scanning Electron Microscopy (SEM) mod. LEO 420. The SEM samples were covered with 250Å of gold using a sputter coater (Agar mod. 108A). The Particle Size (PS) and the Particle Size Distribution (PSD) were measured using the Sigma Scan Pro software (Jandel Scientific) and about 1000 particles were considered in each measure of PSD performed.

3. RESULTS SECTION

Some preliminary experiments were performed using binary systems (EtOH/CO_2 and DMSO/CO_2) of known behavior to obtain some information on the liquid jet formation. These experiments were performed by pressurizing the windowed vessel with CO_2 and then feeding the pure liquid solvent through the injector. When we operated in the two phase conditions; i.e., at conditions in which the binary system liquid-supercritical CO_2 is not completely miscible, we observed the formation of a liquid jet that entered deeply in the fluid phase before its disappearance (Figure 2).

Figure 2. Jet formation.

When we repeated the same experiment in the single phase region; i.e., at pressure and temperature conditions for which the binary system exhibit complete miscibility, the liquid jet was visible only in the immediate proximity of the injector. For example, for the system, DMSO/CO_2 at 40°C and 120 bar the jet was only slightly visible. A further increase of pressure produced its almost complete disappearance.

These results demonstrate that in the single phase region the dissolution of the liquid into the supercritical phase is extremely fast and that the higher is the pressure the faster is the kinetics of liquid dissolution in the SCF.

At this point, we started the study of ternary systems selecting some couples solute/solvent that we had previously tested: YAc/DMSO and YAc/MeOH representative of successful micronization and PNS/MeOH representative of problematic micronization.

When we performed YAc experiments with DMSO or MeOH at conditions of complete miscibility (for example 120 bar, 40 °C), we observed the immediate formation of snow-like solid particles in correspondence of the injection system (Figure 3). The solid particles progressively occupied the whole volume of the precipitator and tended to accumulate prevalently on the bottom of the vessel (on the stainless steel frit). The formation of solids was the faster the higher the operating pressure. We observed in all the cases one clear supercritical phase from which YAc precipitated.

Figure 3. Solute precipitation.

Part of the solid remained in suspension in the fluid phase and deposited prevalently on the side walls and on the quartz windows during the depressurization of the precipitator at the end of the experiments. The solid particles were, then, collected and analyzed by SEM and XRD. As expected from the previous experiments, these particles were amorphous and spherical. An example of such particles is reported in Figure 4.

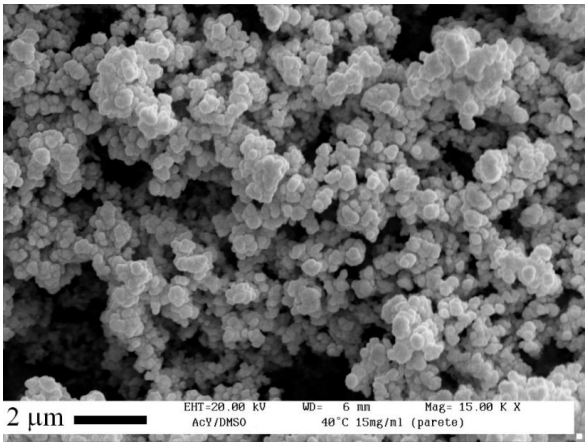

Figure 4. SEM image of micronized YAc at 120 bar, 40°C and 15 mg/ml DMSO.

When we tested the ternary system PNS-MeOH-CO_2, we observed the immediate formation of two phases almost as soon as we started the injection of the liquid solution. They were evidently a supercritical rich phase and a liquid rich phase; the second one occupied the bottom part of the vessel. There was a neat separation between the two phases represented by a meniscus. The relative quantities of the two phases modified continuously until the steady-state concentration was obtained in the vessel. After the attainment of stationary conditions, we observed no further variation of the level of the interface. The relative quantities of the two phases were influenced, at a fixed temperature, by the pressure of the system and by the ratio (R) between the supercritical flow rate and the liquid flow rate. We observed that the higher was the pressure, the higher was the level occupied by the liquid rich phase. Moreover, we observed that increasing R up to 400 the liquid phase occupied a very small volume operating at 85 bar, 40°C and 1 mg/ml.

From the point of view of the precipitated particles, we observed a solute partitioning between the two phases since precipitation occurred from both the fluid and the liquid rich phase. Particles collected were amorphous or crystalline (Figure 5) depending on the precipitation from the fluid or the liquid rich phase, respectively.

Occasionally we observed the formation of three, four and even five different phases along the precipitator, characterized also by neat or evanescent interfaces. We noted the presence of definite interfaces when liquid rich phases were involved and of evanescent interfaces between two fluid rich phases.

A previously proposed model of SAS precipitation describes the process hypothesizing that liquid droplets in contact with supercritical CO_2 rapidly expand due to CO_2 penetration in the droplet. When, on the expanding droplet surface, supersaturation occurs, solute nanoparticles start to precipitate; the dried droplet then explodes generating many particles (one droplet multiple particles model). This model seems further supported by our results. Indeed, the observations about the liquid jet formation in the windowed vessel and its almost immediate disappearance in the single phase region confirm that the kinetics of liquid dissolution in the SCF phase is very fast due to very fast mass transfer. The immediate formation of interfaces between different phases also confirms the exceptional rapidity of mass transfer. These results also mean that the limiting step of the precipitation is not the mass transfer but the thermodynamics; i.e., vapor liquid equilibria (VLEs) at high pressure condition the process evolution.

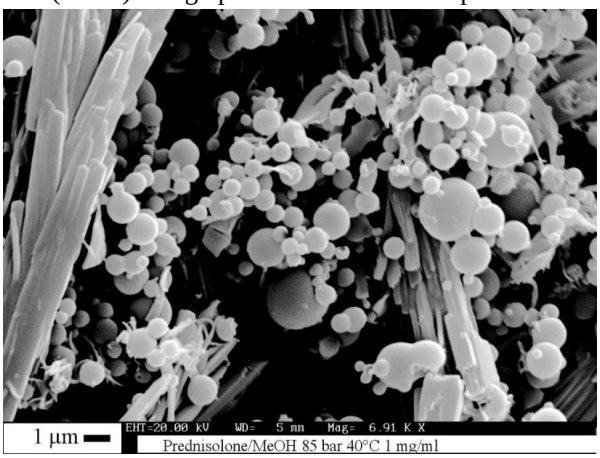

Figure 5. SEM image of micronized PNS at 85 bar, 40°C and 1 mg/ml MeOH.

Our experiments confirm that, when the ternary system maintains the VLE binary behavior, a successful micronization is obtained with the formation of micrometric or sub-micrometric particles. They are amorphou confirming that the process is very fast and does not allow the organization of solids in an ordinate form (crystals).

If the interactions induced by the presence of a solute in the liquid/SCF system generate the appearance of two or more phases, they interfere with the precipitation process. Particles precipitated from liquid rich phases are crystalline according to the ordinary solid formation process from a liquid phase.

We can try to explain the observed behaviors using a triangular representation. A ternary system can be represented by a triangle; the three vertices represent the three pure components, the axes represent two-component systems, whereas the internal areas represent mixtures of the three components. The lines connecting points in equilibrium along the phase boundaries are called tie-lines.

In the attempt to represent the SAS operating point in the ternary diagram, the following considerations have to be taken into account. The liquid solution is obviously injected at a concentration lower than the solubility limit; we hypothesize that the solid and the SCF are immiscible and that the liquid and the SCF are perfectly miscible. During the SAS process, the operating point is on the connection line between the pure CO_2 vertex and the solid-liquid solution line. The exact position on the operating line is given by the ratio R between the antisolvent and the solution flow rate calculated using the lever rule.

Accepting these assumptions, we have a successful precipitation in the case of a binary-like behavior; in this case, the tie-line related to the operating point in the ternary diagram ends on the solute vertex and on the liquid-SCF axis. Therefore, we have the formation of a pure solid and of a fluid phase located on the liquid-SCF axis that does not contain solute (Figure 6). When the interaction among the three components modifies the binary

behavior liquid-SCF it is, for example, possible the solute partitioning between two phases due to an enlargement of the region of miscibility between liquid and SCF due to the presence of solute (Figure 7).

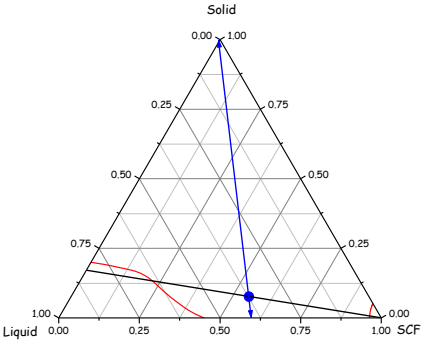

Figure 6. Triangular representation of the successful SAS precipitation.

It is, however, possible to change the operating conditions to improve the precipitation process. The parameters that can modify the high pressure equilibria are temperature, pressure and the concentration of the ternary system.

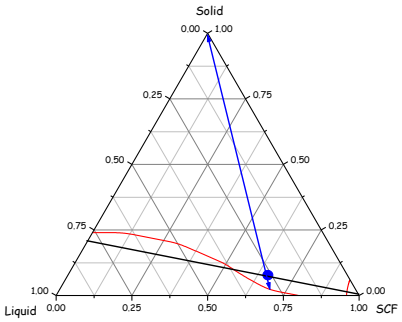

Figure 7. Triangular representation of solute partitioning during a SAS precipitation.

For example, once fixed pressure and temperature, increasing the SCF flow rate and, as a consequence, the antisolvent concentration, the operating point moves towards the SCF vertex. The new operating point could be located on a tie-line that produces again the complete splitting of the solid from the liquid-SCF mixture as in the case of Figure 6 and successful micronization will be produced.

4. CONCLUSIONS

The use of a windowed vessel produced semi-quantitative indications, but they seem very important to understand the precipitation behavior during SAS. The major results are that thermodynamic constraints control the evolution of the precipitation process, due to the very fast mass transfer processes that characterize the process. Further studies are programmed for the next future to characterize other multiphase behaviors and to search for VLE regions that allow the micronization even in the presence of these behaviors.

5. REFERENCES

[1] Gallagher P.M., Coffey M.P., Krunokis V.J., Hillstrom W.W., Gas anti-solvent recrystallization of RDX: Formation of ultra-fine particles of a difficult-to-comminute explosive, *The Journal of Supercritical Fluids*, 5, 2, 130-142, **1992**.

[2] De Marco I., Prosapio V., Cice F., Reverchon E., Use of solvent mixtures in supercritical antisolvent process to modifyprecipitates morphology: Cellulose acetate microparticles, *The Journal of Supercritical Fluids*, 83, 153-160, **2013**.

[3] De Marco I., Reverchon E., Nanostructured cellulose acetate filaments produced by supercritical antisolvent precipitation, *The Journal of Supercritical Fluids*, 55, 1095-1103, **2011**.

[4] Vorobei A.M., Pokrovskiy O.I., Ustinovich K.B., Parenago O.O., Savilov S.V., Lunin V.V., Novotortsev V.M., Preparation of polymer - Multi-walled carbon nanotube composites with enhanced mechanical properties using supercritical antisolvent precipitation, *Polymer*, 95, 77-81, **2016**.

[5] De Marco I., Rossmann M., Prosapio V., Reverchon E., Braeuer A., Control of particle size, at micrometric and nanometric range, using supercritical antisolvent precipitation from solvent mixtures: Application to PVP, *Chemical Engineering Journal*, 273, 344-352, **2015**.

[6] Sacchetin P.S.C., Setti R.F., Rosa P.D.T.V.E., Moraes A.M., Properties of PLA/PCL particles as vehicles for oral delivery of the androgen hormone 17α-methyltestosterone, *Materials Science and Engineering C*, 58, 870-881, **2016**.

[7] Reverchon E., De Marco I., Della Porta G., Tailoring of nano- and micro-particles of some superconductor precursors by supercritical antisolvent precipitation, *The Journal of Supercritical Fluids*, 23, 81-87, **2002**.

[8] Karim F.T., Ghafoor K., Ferdosh S., Al-Juhaimi F., Ali E., Yunus K.B., Hamed M.H., Islam A., Asif M., Zaidul I.S.M., Microencapsulation of fish oil using supercritical antisolvent process, *Journal of Food and Drug Analysis*, 25(3), 654-666, **2017**.

[9] Kondrat S.A., Smith P.J., Wells P.P., Chater P.A., Carter J.H., Morgan D.J., Fiordaliso E.M., Wagner J.B., Davies T.E., Lu L., Bartley J.K., Taylor S.H., Spencer M.S., Kiely C.J., Kelly G.J., Park C.W., Rosseinsky M.J., Hutchings G.J., Stable amorphous georgeite as a precursor to a high-activity catalyst, *Nature*, 531(7592), 83-87, **2016**.

[10] Wang Y., Wang Y., Yang J., Pfeffer R., Dave R., Michniak B., The application of a supercritical antisolvent process for sustained drug delivery, *Powder Techonology*, 164, 2, 94-102, **2006.**

[11] García-Casas I., Montes A., Pereyra C., Martínez de la Ossa E.J., Co-precipitation of mangiferin with cellulose acetate phthalate by supercritical antisolvent process, *Journal of CO2 Utilization*, 22, 197-207, **2017**.

[12] Djerafi R., Swanepoel A., Crampon C., Kalombo L., Labuschagne P., Badens E., Masmoudi Y., Supercritical antisolvent co-precipitation of rifampicin and ethyl cellulose, *European Journal of Pharmaceutical Sciences*, 102(1), 161-171, **2017**.

[13] Alias D., Yunus R., Chong G.H., Che Abdullah C.A., Single step encapsulation process of tamoxifen in biodegradable polymer using supercritical anti-solvent (SAS) process, *Powder Technology*, 309, 89-94, **2017**.

[14] Arango-Ruiz Á., Martin Á., Cosero M.J., Jiménez C., Londoño J., Encapsulation of curcumin using supercritical antisolvent (SAS) technology to improve its stability and solubility in water, *Food Chemistry*,
258, 156-163, **2018**.

[15] Prosapio V., De Marco I., Reverchon E., Supercritical antisolvent coprecipitation mechanisms, *The Journal of Supercritical Fluids*, 138, 247-258, **2018.**

[16] Campardelli R., Reverchon E., De Marco I., Dependence of SAS particle morphologies on the ternary phase equilibria, *The Journal of Supercritical Fluids*, 130, 273-281, **2017**.

© 2018 by the authors. This article is an open access article distributed under the terms and conditions of the Creative Commons Attribution license (http://creativecommons.org/licenses/by/4.0/).